Al-Qadisiyah JournalFor Engineering Sciences 18 (2025) 281 – 289

Contents lists available at: http://qu.edu.iq

Al-Qadisiyah Journal for Engineering Sciences

Journal homepage: https://qjes.qu.edu.iq

Research Paper

Synthesis and study of carbon-based magnetic catalysts for biodiesel production

Ali Flayyih Hasan[1]✉, ***Ahmed A. Obaid***[1], ***Omid Amanzadeh***[2], ***and Falah Abdulhassan***[3]

[1]*Department of Chemical Engineering, Faculty of Engineering, University of Al-Qadisiyah, Al-Diwaniya 58002, Iraq.*
[2]*Department of Chemical Engineering, Babol Noshirvani University of Technology, Babol, Iran.*
[3]*Department of Mechanical Engineering, Trafford College Group, Manchester, United Kingdom.*

ARTICLE INFO

Article history:
Received 22 September 2024
Received in revised form 02 February 2025
Accepted 15 July 2025

keyword:
Activated carbon
Calcination
FAME
Fossil fuels
Nanostructured catalysts

ABSTRACT

Biodiesel is a promising alternative to conventional fossil fuels, so effective catalysis is essential to enhance the efficiency and selectivity in biodiesel production. This article discusses one of the methods used to synthesize these catalysts and their effectiveness in biofuel production. A catalyst was synthesized from palm frond waste, which is abundant in Iraq. Palm frond dust acquired magnetic properties by adding iron (III) chloride by the impregnation method. Palm frond dust was carbonized for 3 h at 700 $C°$and then sulfonated using ($H2SO4$) depending on variable factors such as reaction time, temperature, and acid concentration. The change of these factors on the acidity value of the catalyst was studied. The catalyst was characterized using techniques such as FTIR, SEM, acid value, and BET. The study successfully prepared an effective magnetic catalyst with the possibility of recovery due to its magnetic properties. The surface area determined by BET was 585.12 m^2/g, indicating a high specific surface area value. The highest expected acid value was 4.23 $mmol/g$ at a reaction time of 2.6 $h°$, a temperature of 50 $C°$, and a concentration of 10 M.

1. Introduction

The worldwide problem of energy security has arisen due to the escalating energy demand resulting from the growing human population and the dominating reliance on fossil fuels for transportation [1, 2]. World reliance on fossil fuels has led to significant energy shortage issues and ecological degradation. The aforementioned issues have resulted in a pressing requirement for a viable and enduring alternative bioenergy source [3]. A wide range of renewable energy sources, such as biomass, solar, wind, and nuclear power, have the potential to substitute fossil fuels [4]. Renewable fuels have generated significant attention, leading to extensive research on developing improved biofuels derived from oil crop feedstock ,[5]. Biodiesel is a promising sustainable fuel proposed as a viable substitute for fossil diesel [6]. The procedures of product separation and catalyst recovery in conventional biodiesel manufacture are characterized by significant energy consumption and economic inefficiency. Biodiesel use has increased 15-fold since 2004 [7]. Biodiesel often exhibits improved combustion efficiency, less emissions, and notable lubricating properties. The adverse effects of global warming, resulting from the increasing usage of fossil fuels, have become significant elements propelling the global progress of biodiesel [8]. Biodiesel is a potential and valuable renewable fuel because of its inherent ability to biodegrade, renewable characteristics, and beneficial environmental effects. It significantly reduces the release of carbon dioxide and sulfur. Combusting biodiesel has decreased net CO2 e- missions by 78%, carbon monoxide (CO) emissions by 46.7%, and the discharge of polluting particles such as NO3, SO4, organic compounds, ash particles, dust, and metals by 66.7%. Moreover, it reduces the quantity of uncombusted hydrocarbon emissions [9]. it has The potential to greatly mitigate the impacts of global warming. Furthermore, biodiesel may be employed in conventional engines by combining it with petroleum diesel in a certain proportion, such as 10% biodiesel and 90% petroleum diesel. Based on its chemical composition, Biodiesel is classified as a fatty acid methyl ester (FAME) [10]. Biodiesel is produced by reacting fatty acids with methanol in the presence of a catalyst [11]. On the other hand, the non-catalytic process often requires a longer duration and results in a lower amount of product. Esterification and transesterification chemical processes are the most effective techniques for creating biodiesel [12]. Transesterification is a chemical process in which vegetable oil reacts with alcohol, with the help of a catalyst, to form fatty acid alkyl ester. Glycerol is also created as a byproduct. Various raw materials have been documented for biodiesel manufacturing, encompassing food oils, non-edible oils, and microalgae-derived oils [13]. As for catalysts used in production, the industry has mostly used uniform base catalysts for many years. In literature, sodium hydroxide (NaOH) and potassium hydroxide (KOH) are commonly cited as base catalysts. Sodium or potassium methoxide may be easily produced by dissolving KOH in methanol due to its high solubility [14]. Utilizing homogeneous base catalysts allows for a substantial synthesis of methyl esters under gentle reaction conditions, leading to a reduced reaction time. While homogeneous base catalysts offer several benefits, a significant amount of free fatty acids (FFA) in oil feedstock might cause undesired saponification side reactions. These reactions result in the generation of a considerable amount of soap by-products, which hinder the subsequent separation and purification processes [15]. However, homogeneous acid catalysts like sulphuric acid, hydrochloric acid, and phosphoric acid are suitable for feedstock with a substantial quantity of free fatty acids (FFA), such as waste frying oil and unrefined vegetable oil [16]. These catalysts have enhanced resistance to elevated amounts of free fatty acids (FFA) and water. Homogeneous acid catalysts yield a substantial amount of product, but at a somewhat slower reaction rate than homogeneous base catalysts [17]. Although homogeneous acid catalysts exhibit high reactivity, their strong acidity leads to significant problems such as pipeline corrosion and environmental pollution.

*Corresponding Author.
E-mail address: alifalyihhassan@qu.edu.iq ; Tel: (+964 780-099-5423) (Ali Hasan)

https://doi.org/10.30772/qjes.2024.150386.1259
2411-7773

Nomenclature

BBD	Box-Behnken Design	*H*	Highly significant
DOE	Design of experiments	*S*	Significant
FTIR	Fourier Transform-Infrared Spectroscopy	*SEM*	Scanning Electron Microscope

Additionally, extracting the dissolved homogeneous catalyst from the reaction mixture necessitates extra washing steps, which poses challenges for both recovery and reusability [16]. Heterogeneous catalysts are increasingly used in biodiesel production due to their ability to remain unaltered and reusable, resulting in higher catalytic efficiency [18]. Magnetic materials have gained attention as effective catalyst supports due to their magnetic properties, enabling efficient separation of solid catalysts with minimal mass loss. Magnetic separation eliminates the need for labor-intensive separation and recovery methods and significantly minimizes the loss of solid catalysts during the separation process [19].The primary magnetic materials used in solid catalyst production include monodisperse nanocrystals like Fe3O4 and $-Fe2O3$ and ferrite microspheres like $MFe2O4$. Techniques for producing magnetic nano-materials include coprecipitation, thermal breakdown, micro emulsion-based synthesis, and hydrothermal and solvothermal synthesis [19].

Magnetic carrier materials typically include monodisperse magnetic nanoparticles and magnetic nanocomposites. Monodisperse nanocomposites modified with minuscule organic molecules are superior carriers for producing solid catalysts, as they have uniform particle sizes and enhanced magnetic properties. However, magnetic nanoparticles tend to aggregate into large clusters due to their high surface energy and magnetic dipole attractions, hindering the uniform dispersion of the proposed magnetic catalyst in the reaction mixture. Applying a protective coating on magnetic nanoparticles could impede their magnetic aggregation and improve their chemical stability [20].

The use of heterogeneous catalysts in biodiesel generation has gained significant attention due to their ability to preserve the substance's integrity, allowing for easy separation and reuse. These catalysts demonstrate superior catalytic efficacy compared to homogeneous catalysts [18]. Studies have shown that using a CaO catalyst as a heterogeneous catalyst can reduce the duration of biodiesel synthesis and effectively catalyze oils with high acid values. They are non-corrosive, can be easily separated and recycled without the need for regeneration procedures, and can be reused up to 30 times for transesterification and eight times for esterification without any noticeable decrease in catalytic activity [21]. Various heterogeneous catalysts, such as metal oxide, mixed oxide, transition metal oxide, ion exchange resin, carbon-based catalysts, and zeolite, can be employed in a base-catalyzed process [22]. However, these catalysts frequently possess disadvantages such as costly production, significant toxicity, susceptibility to leaching, restricted acid sites on the surface due to extreme microporosity, and a lack of environmental compatibility [23].

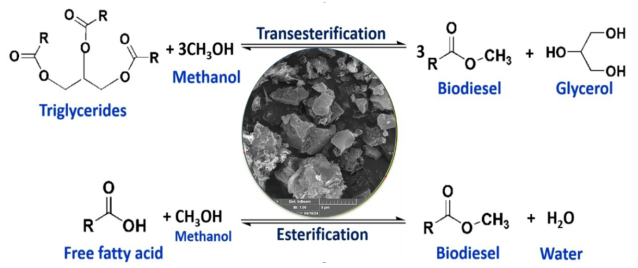

Figure 1. Schematic illustration of the transesterification and esterification reactions for biodiesel production using the magnetic solid catalyst.

Biomass resources are commonly utilized as a feasible feedstock for the ecologically sustainable production of biofuels [24]. Incorporating various catalysts derived from biomass into the process offers a feasible and eco-friendly choice, Fig. 1. To resolve these inconsistencies, magnetic materials, such as external magnetic fields or nanoparticles, have been investigated as catalytic supports for the transesterification process. Magnetic nanoparticle catalysts may be uniformly dispersed throughout reaction mixtures, augment the accessibility of reactants by expanding the surface area, and can be reused several times with minimal reduction in catalytic efficacy [25]. Magnetic catalysts serve as intermediaries that connect both homogeneous and heterogeneous catalysts, possessing the characteristics of both homogeneous catalysts (displaying high reactivity) and heterogeneous catalysts (allowing for facile separation) [16]. Thus, solid acid catalysts have been widely studied because they do not present corrosion problems and can be recovered and reused in the reaction cycle [26]. This research specifically examines the process of creating magnetic solid acid carbon-based catalysts for producing biodiesel. Characterizing the catalyst by the use of SEM, BET surface analyzer, and FTIR to identify the ideal conditions for synthesizing a catalyst.

2. Material and method

Palm fronds, Iron (III) Chloride ($FeCl3$) will be used to attract the catalyst magnetically, and acid $H2SO4$ will introduce the active group. Apply mathematical modeling and statistical analysis to the improvement process.

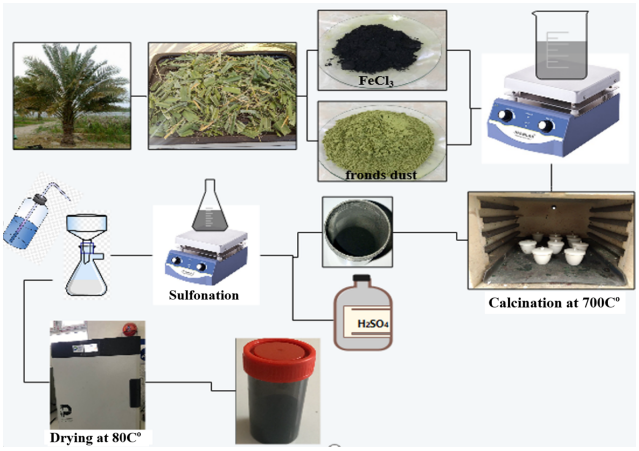

Figure 2. Preparation of carbon-based magnetic from palm fronds.

2.1 Cataltst preparation

Preparation of Support: Fronds from palm trees were gathered and sun-dried for at least three days, Fig. 2. Next, they were divided into smaller pieces and blended. Next, a $300\mu m$ sieve was used to filter the powder. Producing Magnetic Support: Place 20 gm of iron chloride in 250 ml of distilled water and add 20 g of the prepared powder. Mix using a hotplate steer at 200C°while stirring at 200 rpm for 3 hours and drying at 80C°for 24 hours. Calcination of Magnetic Support in the Furnace at (700C°) for 3 hours without air. A magnetic catalyst was prepared using Minitab following the sulphonation condition, as shown in Table 1. The catalysts were compared based on their acid density with different sulphonation time, temperature, and concentration parameters.

Table 1. Real and coded process variables for the effect of different parameters on the sulphonation process of the catalysts.

Name	Code	Law (-1)	Middle (0)	High(+1)
Time (h)	X_1	1	2	3
Temperature (C°)	X_2	50	100	150
Concentration (M)	X_3	0	5	10

3. Catalytic characterization

An approach that is frequently used to investigate and characterize the surface functional groups and vibrational bonds that are present on catalyst powder is Fourier transform infrared spectroscopy or FT-IR. Using the KBr pellet method, a Bruker Vertex80 spectrometer was used to analyse the powdered catalyst sample over a wavenumber range of 400–4000 $cm-1$. The morphological features and crystal sizes of the samples were examined using a field emission scanning electron microscope (FE-SEM), specifically a $MIRA3$ model from TESCAN, USA, operated at an accelerating voltage of 15 kV. To minimize charging effects during imaging, the samples were coated with a thin layer of gold prior to being photographed in the microscope [27].

3.1 Scanning electron microscope (SEM)

Scanning Electron Microscopy (SEM) plays a crucial role in surface analysis, particle examination, and material failure assessment in catalysts. Surface

morphology and the structural changes at the micro- and Nano-scale levels can be analyzed in detail. Through Fig. 3, it can be noticed that, after the addition of iron chloride, the surface roughness considerably increases. The roughening of the surface may be associated with the chemical and physical absorption processes of iron chloride molecules. After calcination, further observation is made of the increase in the number of cracks and pores in the material's structure. Such a behavior occurs due to the process of volatilization, in which several chlorine, oxygen, and other volatile materials come out of the material. The roughening and the creation of cracks and pores after calcination are important to prove that surface morphology and material structure have been changed considerably, which is important to determine if a catalyst material is good enough or not in terms of results and life [28]. In Fig. 4 shows slight changes in the shape and distribution of particles as a result of sulfonation of the catalyst with acid, with a clear change in the pore size, which affects the active surface of the catalyst and the accessibility of the reactive materials [29].

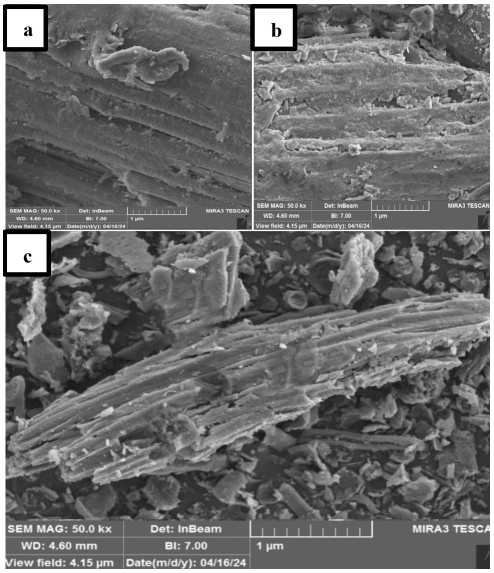

Figure 3. SEM Images of the frond dust (a) before adding FeCl3, (b) after adding FeCl3, and (c) Magnetic Support After Calcination.

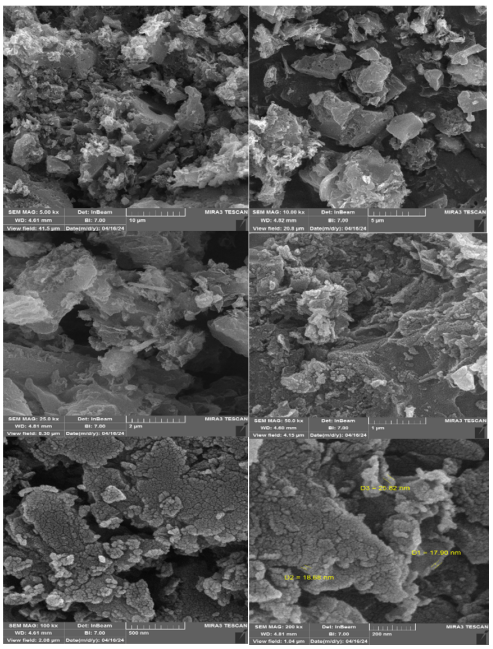

Figure 4. FESEM Images of the magnetic solid catalyst after the Sulphonation process.

3.2 Fourier transform infrared (FTIR) spectroscopy

Their attachment to the magnetic catalyst is a critical step in enhancing catalytic performance. It is real that iron oxides display magnetic properties and catalytic activity; therefore, they are pivotal components in various heterogeneous catalytic reactions.

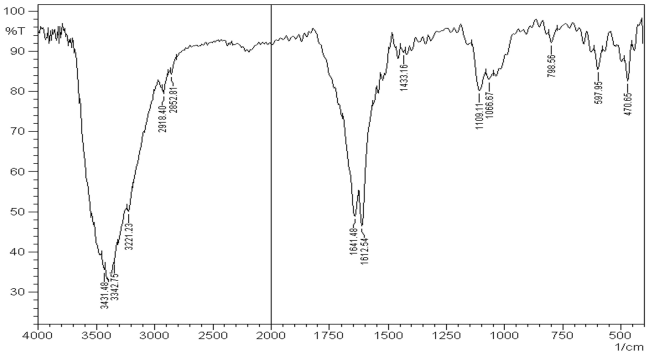

Figure 5. FTIR of Front Dust.

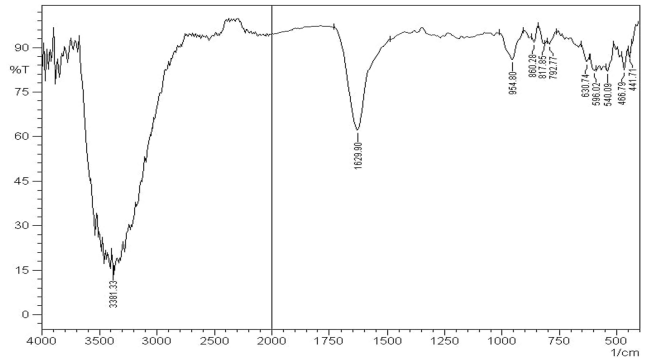

Figure 6. FTIR of Front Dust After Addition FeCl3.

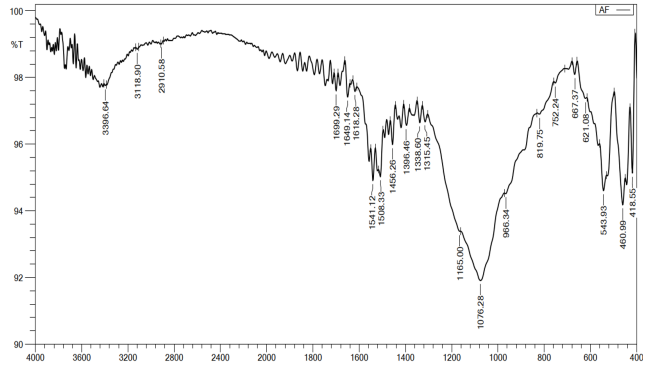

Figure 7. FTIR of Magnetic Catalyst.

Table 2. The potential functional groups that can be identified using FTIR.

Wavenumber, (cm^{-1})	Possible bond group
2800 – 3500	$O-H$
2800 – 3000	$C-H$
1500 – 1650	$C=O$
1400 – 1600	$C-O$
1000 – 1300	$S-O$
500 – 600	$Fe-O$
< 400	$Fe/Fe-S$

The iron oxides get attached to the catalyst support through proper synthesis methodologies [30]. The Fig. 5, Fig. 6 and Fig. 7 are well characterized

by a range of analytical techniques, among which Fourier-transform infrared spectroscopy stands as one of the main methods applied. FTIR spectroscopy helps in the determination of specific chemical bonds and functional groups on the catalyst surface, Table 2. For the (Fig. 5, Fig. 6 and Fig. 7) of iron oxide above-mentioned, characteristic absorption bands seen due to metal-oxygen vibrations in the FTIR spectrum clearly indicate successful incorporation. Further spectral shifts or intensity changes in some regions also determine the nature of bonding between the iron oxides and the catalyst support, thus further supporting the attachment mechanism.

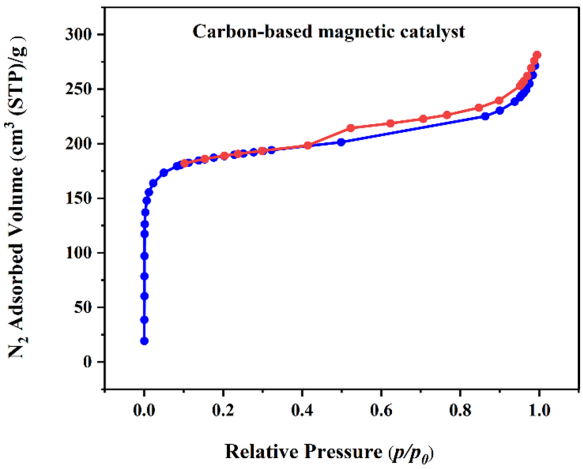

Figure 8**.** Shows the nitrogen adsorption-desorption isotherms of the samples studied.

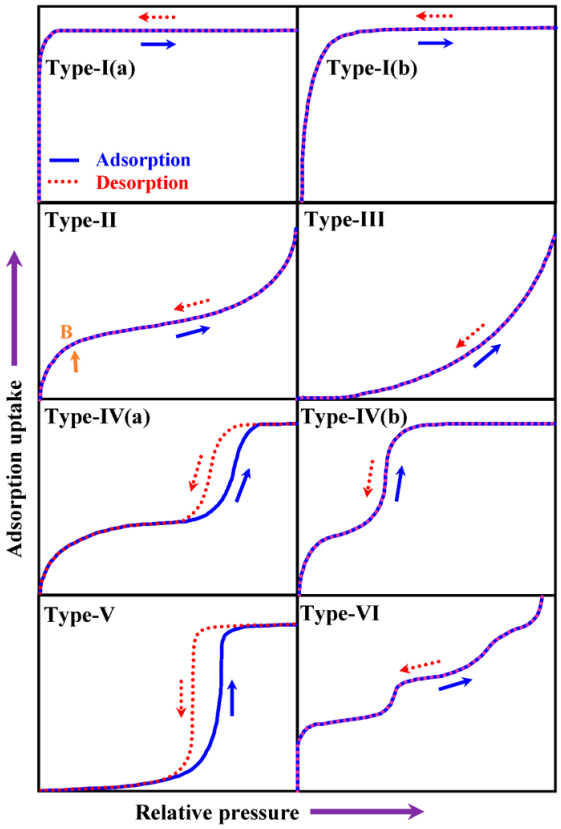

Figure 9**.** Classification of physisorption isotherms, [31].

Moreover, catalytic activity and selectivity can be further enhanced by the combination with an amorphous carbon support bearing $-SO3H$ groups. With the presence of the $-SO3H$ functional group in this work's catalyst, it makes it very acidic, able to promote most acid catalysis, such as esterification, hydrolysis, and dehydration. The sulphonation process involves treating the carbon support with sulphonic agents through which the surface of the carbon gets covalently attached by the $-SO3H$ groupsThis fact, namely, the incorporation of the $-SO3H$ group onto the carbonaceous surface, is further supported by FTIR analysis following sulphation events that can be identified by characteristic absorption bands corresponding to sulphonic acid functionality. The presence in the FTIR spectrum of peaks related to stretching vibrations and bending modes of $S-OH$ was indicative of the presence of sulfonic acid moieties at the catalyst surface [32]. In brief, the in-depth description of the magnetic catalyst in terms of iron oxide attachment and $-SO3H$ functionalisation highlights the synergistic activity between materials chemistry and catalysis. Using advanced analytical tools, intricate structural features and chemical functionalities can be explained, which optimise catalytic efficiency and facilitate the design of tailor-made catalysts for a wide range of applications. Finding functional groups is one area in which FTIR is really helpful. The catalyst's performance is largely dependent on its functional groups since the catalyst under study is acid-functionalized carbon. The catalyst's primary association is with $-SO3H$ groups, which are significant acid sites. In addition to the $-SO3H$ group, other groups generated during the sulphonation process were the $-OH$ and $-COOH$ groups The study presented in Table 2 displays all the relevant functional groupings [32].

3.3 N_2 Adsorption-desorption isotherm analysis

Nitrogen adsorption-desorption isotherms are widely applied to study the textural properties of porous materials. From these isotherms, data about the amount of nitrogen gas adsorbed at different pressures are obtained, and then different parameters related to the surface area, pore volume, and pore size distribution can be calculated. Figure 8 shows the nitrogen adsorption-desorption isotherms of the samples studied, while the pore size distribution plots, Fig. 9 can supply information about the pore dimensions of the material. Figure 8 N2 adsorption-desorption isotherms of carbon-based magnetic catalyst at standard temperature and pressure. The adsorption branch (blue circles) and the desorption branch (red circles) of the isotherm show typical type IV isotherms, which are characteristic of mesoporous materials [33].

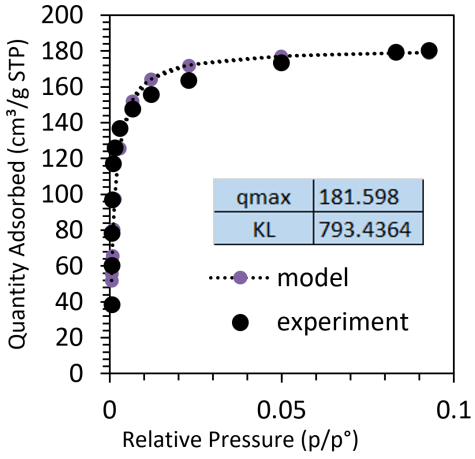

Figure 10**.** Langmuir adsorption isotherm.

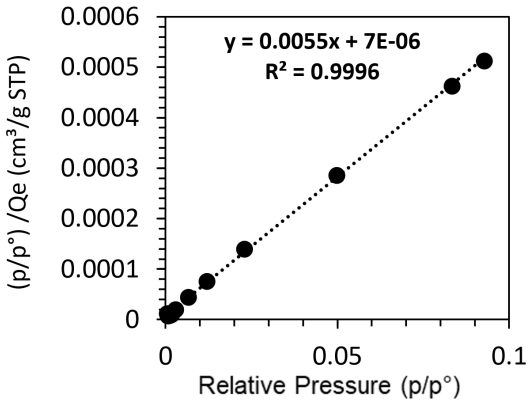

Figure 11**.** Linearized Langmuir adsorption Isotherm.

At relative pressures $P/P_o < 0.1$, a sharp increase in the nitrogen uptake is observed, as a result of micropore filling. As the relative pressure increases ($0.1 < P/P_o < 0.8$), the adsorption isotherm slope decreases, due to adsorption in the mesopores. The volume of adsorbed nitrogen slowly increases in this range from ca. 50 cm^3/g to ca. 200 cm^3/g. At high relative pressures ($P/P_o > 0.8$), the isotherm shows a hysteresis loop, due to capillary condensation in the mesopores. The ending of the hysteresis loop at high pressures indicates that the mesopores are uniform. The total volume of nitrogen adsorbed is about 250 cm^3/g at $P/P_o = 1.0$. On the other hand, the Brunauer-Emmett-Teller (BET) analysis gives additional information about the surface properties of the catalyst. The surface area determined by BET is 585.12 m^2/g, indicating a high specific surface area value. Because there are more active sites available for the reaction, a high surface area is a fundamental requirement for catalytic activity. There is a 436.35 m^3/g micropore area and a 148.76 m^2/g mesopore area. These numbers imply that the surface area is primarily contributed by the micropores. The catalyst has a total pore volume of 0.375 cm^3/g, of which 0.226 cm^3/g is mostly attributed to micropores and 0.148 cm^3/g to mesopores. These results verify the micro/mesoporous nature of the catalyst, which promotes reactant molecule accessibility and diffusion and enables an effective catalytic process. The porous structure of the carbon-based magnetic catalyst, which exhibits a mesoporous character with a high value of specific surface area and pore volume, is revealed by the adsorption-desorption isotherms. These properties, which improve reactant molecule accessibility and diffusion, are advantageous for catalytic applications [34]. There are six types of adsorption isotherm models (types I, II, III, IV, V, and VI) based on the shape of the isotherm models as shown in Fig. 9.

The Langmuir isotherm model, Fig. 10, implies that the distribution of reactive groups on the particle surface is uniform and that there is no contact between adjacent particles [35]. The Langmuir equation, derived from gas theory, is widely employed to explain the adsorption of gases onto solids [36]. The Langmuir sorption isotherm is applicable under the following conditions: the solute adsorption occurs in a single layer, the surface has a fixed number of identical sites with a consistent adsorption mechanism, and there is no movement of the adsorbate within the surface plane (Gautam et al., 2014). Equation 1 displays the non-linearized version of the Langmuir isotherm model proposed by Langmuir in 1918.

$$Q_e = \frac{Q_o \times KL \times C_e}{1 + KL \times C_e} \tag{1}$$

Equation 2 represents the linearized version of the Langmuir model, Fig. 11.

$$\frac{C_e}{Q_e} = \frac{1}{KL \times Q_o} + \frac{C_e}{KL} \tag{2}$$

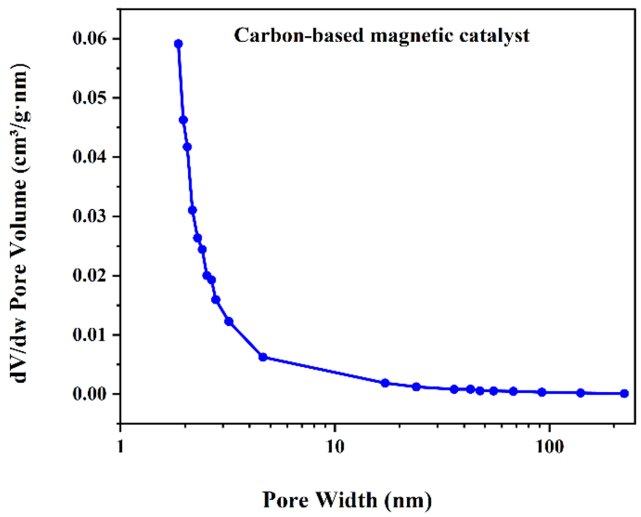

Figure 12**.** Illustrates pore volume changes with pore width for a carbon-based magnetic catalyst.

The variable Q_e represents the maximal adsorption capacity on a monolayer, measured in milligrams per gram (mg/g). The variable KL represents the Langmuir adsorption constant, measured in liters per milligram (L/mg), which is associated with the apparent energy of sorption. In Fig. 12, the BJH graph illustrates pore volume changes with pore width for a carbon-based magnetic catalyst. As the width increases from 1 *nm* to 10 *nm*, there is a sharp drop in pore volume, followed by a slower decline for wider pores. This indicates that there are lots of micropores (less than 2 *nm* wide) and mesopores (2 to 50 *nm* wide) in the catalyst. These pores are key factors, giving the catalyst a large surface area and making it great for catalytic activity. The presence of fewer mesopores is attributed to the slower decrease in pore volume at larger pore widths. These pores contribute less to the surface area but facilitate mass transport within the catalyst. In conclusion, the carbon-based magnetic catalyst possesses a well-defined pore structure with a micro/mesoporous structure, making it suitable for catalytic applications.

The specific BET surface area, total pore volume, and average pore diameter of carbon-based magnetic catalysts synthesis from Palm Fronds were 585.121 m^2/g, 0.375452 cm^3/g, and 2.56666 *nm*, respectively. It is considered one of the most important characteristics that indicate the catalyst's efficiency.

3.4 Acid value of catalyst

For 30 minutes, mix 0.5 from the magnetic catalyst with 20 Ml of 0.1 M NaOH, then filtrate the solution from the catalyst. After that, it was titrated with 0.01 HCl, with a few drops of phenolphthalein added to serve as a color indicator until the mixture lost its hue. The acid density was computed by recording the volume of hydrochloric acid needed to neutralize the solution. The results are shown in Table 4.2.

4. Results and discussions

The parameters listed in Table 1 were followed in preparing the magnetic catalysts. Table 3 was created using the Box-Behnken Design (BBD) surface response method based on the three most important factors that produce the highest acidity value: time (1-3 hours), temperature (50-150C°), and concentration (0-10 M). The optimal catalyst for the esterification process was selected after an acid density test. At least 15 experiments were required to conduct statistical analysis and determine the interaction between the three factors; the results were recorded in Table 4. To investigate the parameters that impact the responses, the experimental data were analyzed using Minitab Design of Experiments (DOE). This method employs techniques to implement specific procedures and monitor the interaction between variables and their results. It serves as a statistical method for planning, conducting, and analyzing experiments, aiming to obtain the maximum amount of information through the minimum number of experiments, thereby reducing time and cost.

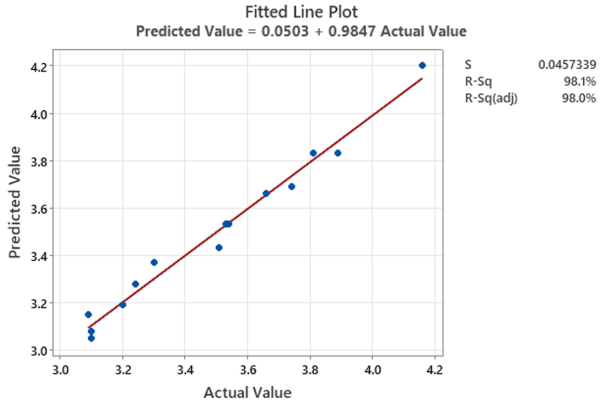

Figure 13**.** Regression Analysis Acid value experimental data versus expected data.

$$Y = B_o + \sum B_i X_i + \sum B_{ii} X_i^2 + \sum\sum B_{ij} X_i X_j + \varepsilon \tag{3}$$

where Y represents the studied responses, X1, X2, and Xq are the operating factors, the total number of operating factors is indicated by q, and Bo-Bij are the regression coefficients, Fig. 13. To investigate the desired responses. In runs 1 to 4, where time varies from 1 to 3 hours and temperature from 50C°to 150C°at a constant concentration of 5M, both increasing time and higher temperatures lead to a slight increase in acid density. For runs 5 to 8, with time varying from 1 to 3 hours and concentration from 0 to 10M at a constant temperature of 100°C, the data show that higher concentration significantly increases acid density. In runs 9 to 12, where temperature varies from 50C°to 150C°and concentration from 0 to 10M at a constant time of 2 hours, higher concentration and lower temperatures result in higher acid

density. Runs 13 to 15, which repeat the conditions of 2 hours, 100C°, and 5M concentration, yield consistent acid density values, indicating the reliability of the experimental setup. Overall, the data suggest that acid density increases with higher concentrations and that both temperature and time have significant, though more complex, effects on the acid density, highlighting the importance of optimizing these variables for desired outcomes in chemical processes. Regression Equation in Uncoded Units Eq.4.

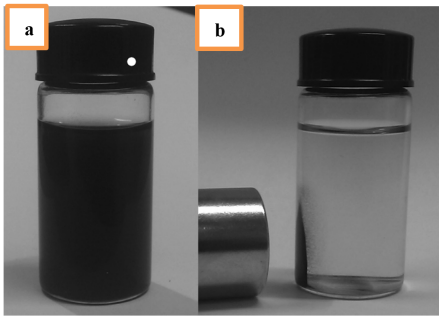

Figure 14**.** Picture of dispersed carbon-based magnetic catalysts in methanol before (a) and after (b) being attracted by an external magnet.

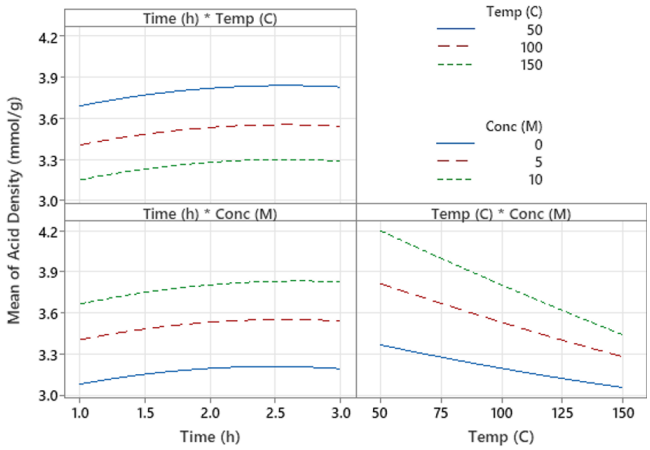

Figure 15**.** Interactions between the response of acid value and operational variables for magnetic catalyst.

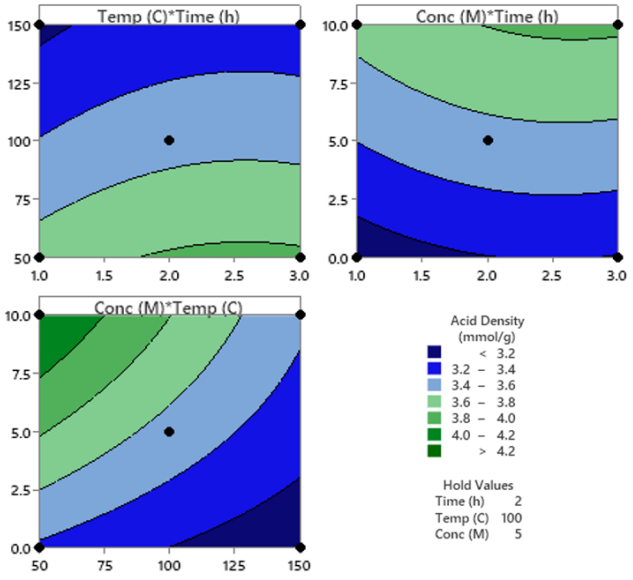

Figure 16**.** The final acid value response vs. the Contour plots of the studied variables of catalysts.

$$Acid\ Density\ (m\ mol/g) = 3.223 + 0.293X_1 - 0.00439X_2 + 0.1137X_3 - \\ - 0.0592X_1^2 + 0.000006X_2^2 - 0.00127X_3^2 + \\ + 0.0025X_1X_3 - 0.00045X_2X_3 \quad (4)$$

Table 5 of ANOVA presents the results of a regression analysis aimed at predicting the acid value for carbon-based magnetic catalysts,Fig. 14, based on various factors, including time, temperature, and concentration. The model employed in this analysis to be statistically significant (P-Value = 0.001), indicating that it effectively captures the relationship between the independent variables and the acid value. Among the linear effects, time, temperature, and concentration all exhibit significant impacts on the acid value, as evidenced by their respective P-Values being less than 0.05. This suggests that variations in these variables directly influence the acid value of the catalysts. Additionally, the quadratic effect of temperature is also found to be significant (P-Value = 0.696), implying that the relationship between temperature and acid value may be non-linear. Examining the two-way interactions, the analysis reveals that the interaction between temperature and concentration is statistically significant (P-Value = 0.028). This indicates that the combined effect of these two variables on the acid value is more complex than their individual linear effects and needs to be accounted for in the model. Despite the model's overall significance and the inclusion of relevant factors, the lack-of-fit is found to be significant (P-Value = 0.004). This suggests that the model may not fully capture all the nuances of the relationship between the variables, and there may be additional factors or higher-order interactions that could further improve the model's predictive ability. The model's goodness-of-fit is assessed through the R^2, adjusted R^2, and predicted R^2 values. The R^2 value of 98.15% indicates that the model explains a substantial portion (98.15%) of the variability in the acid value data. The adjusted R^2 (94.82%) and predicted R^2 (70.45%) values, while lower than the R^2, still suggest a reasonably good model fit and predictive capability, respectively. In summary, this ANOVA analysis provides valuable insights into the factors influencing the acid value of carbon-based magnetic catalysts, identifying significant linear, quadratic, and interaction effects. While the model exhibits good overall performance, the significant lack-of-fit suggests potential room for further improvement by considering additional variables or higher-order interactions. Figure 15 shows the interaction effects of temperature (C°), mass (M), and time (h) on the acid concentration (mmol/g) present when using a magnetic catalyst. This interaction is well illustrated in the three subplots. The relationship between temperature and acidity can be seen in the left subplot. The temperature is shown in blue at 50C°, yellow at 100C°, and green at 150C°. There is a positive correlation between reaction time and acid concentration, as shown by the increase in acid concentration with time at all temperature levels. The acid concentration increases from about 3.3 mmol/g at 0.5 h to about 3.8 mmol/g in 3.0 h at 50C°. At 100C°, the increase over the same period ranges from about 3.5 mmol/g to 4.0 mmol/g. The concentration starts at about 3.7 mmol/g and increases to about 4.2 mmol/g at 150C°. The interaction between concentration and time on acid concentration is shown in the middle subplot. The concentrations shown are 0 M for the blue solid line, 5 M for the red dashed line, and 10 M for the green dashed line. Acid levels increase with time and concentration. At 0 M, it takes three hours to increase the acid concentration from about 3.0 mmol/g to about 3.4 mmol/g. It increases from 3.5 mmol/g to 3.9 mmol/g at 5 M and from 3.9 mmol/g to 4.2 mmol/g at 10 M. The effect of concentration and temperature on acid concentration is shown in the upper right subplot. The concentration of 0 M is the solid blue line, 5 M is the red dashed line, and 10 M is the green dashed line. At all concentrations, acid concentration decreases with increasing temperature. At 0 M, the acid concentration decreases from about 3.8 mmol/g at 50°C to about 3.1 mmol/g at 150C°. These interaction diagrams reveal a complex relationship of acid concentration that is influenced by the interplay of these variables. The findings suggest that although acid concentration is generally positively affected by time and concentration, higher temperatures can have the opposite effect, especially at lower concentrations. The relationship between three important variables, reaction time (h), temperature (C°), concentration (M), and the catalyst's acid density ($m\ mol/g$) is illustrated through a series of contour plots in Fig. 16. The plots make a thorough visual representation of how variations in these variables affect the acid density possible. The contour lines in the top-left plot, which analyses the relationship between temperature and reaction time, show areas with equal acid density. Deeper blue tones denote lower acid densities, which are displayed in green and range from less than 3.2 $m\ mol/g$ to more than 4.2 $m\ mol/g$. An optimal range of acid density around 4.0 to 4.2 $m\ mol/g$ is suggested by the notable increase in acid density as the temperature rises from 50°C to 150°C and the reaction time increases from 1 to 3 hours. This is indicated by the transition from blue to green areas. The relationship between reaction time and concentration is examined in the top-right plot. The contour gradients

indicate that an increase in reaction time from 1 to 3 hours gradually increases the acid density from 3.2 to 3.8 $m\ mol/g$ at lower concentrations (below 2.5 M). However, when the concentration rises above about 7 M, the acid density significantly increases and exceeds4.2 $m\ mol/g$, particularly when the reaction time is longer than two hours. The temperature-concentration relationship is represented visually in the bottom-left plot.

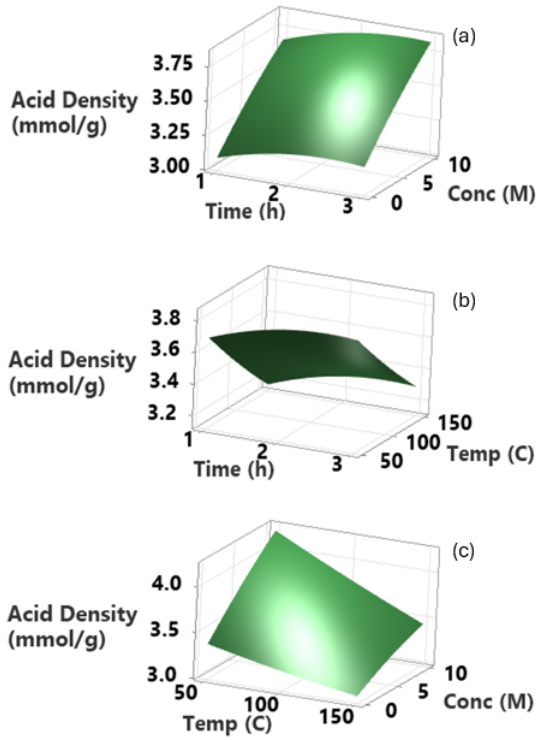

Figure 17. The final acid value response vs. the surface plots of the studied variables of catalysts. The hold values are Time is 2h, temp. 100C°, and Conc 5M.

Table 3. Effect of Different Parameters on the Acid Density of the Catalysts.

Run	Time (h)	Temperature (C°)	Concentration (M)	Acid Density ($m\ mol/g$)
1	1	050	05	3.74
2	3	050	05	3.89
3	1	150	05	3.09
4	3	150	05	3.24
5	1	100	00	3.11
6	3	100	00	3.23
7	1	100	10	3.66
8	3	100	10	3.81
9	2	050	00	3.32
10	2	150	00	3.10
11	2	050	10	4.16
12	2	150	10	3.51
13	2	100	05	3.53
14	2	100	05	3.54
15	2	100	05	3.53

According to the plot, in order to achieve significant acid densities at lower temperatures (around 50C°), concentrations higher than 7.5 M are required. The concentration needed for the ideal acid density reduces as the temperature approaches 150C°. Temperature and concentration are inversely correlated, as the highest acid densities, above 4.2 $m\ mol/g$, are found in areas where both parameters are maximized. The maximal acid density is obtained by precisely combining variables, as indicated by the black dots in each plot. These dots represent the ideal conditions derived from the experimental data. At 150C°, 10 M concentration, and 3 hours of reaction time, for example, an ideal acid density of about 4.2 $m\ mol/g$ is reached. By enabling the identification of the optimal parameters for optimizing efficiency, these contour plots are crucial for comprehending the complex effects of reaction conditions on catalyst performance. The provided Fig. 17 showcases a set of three-dimensional surface plots illustrating the relationship between acid density (measured in mmol/g) and three experimental variables: time (hours), temperature (C°), and concentration (M). Each plot demonstrates how two of these variables influence acid density while holding the third variable constant at specific values. The hold values are defined as follows: time at 2 hours, temperature at 100C°, and concentration at 5 M. The first plot shows the effects of time and temperature on acid density with concentration held constant at 5M. Acid density gradually increases with time, indicating that longer reaction durations favor the formation of acidic species. A substantial rise in acid density with increasing temperature suggests that higher temperatures promote the formation of strongly acidic sulfonic groups and other acidic oxygen functional groups. The second plot shows the effect of time and concentration on acid density, with temperature set at 100C°.

Table 4. Experimental results of acid value vs Predicted Value.

Run	Actual Value	Predicted Value	Residual
1	3.74	3.69	+0.05
2	3.89	3.83	+0.06
3	3.09	3.15	-0.06
4	3.24	3.28	-0.04
5	3.10	3.08	+0.02
6	3.20	3.19	+0.01
7	3.66	3.66	+0.00
8	3.81	3.83	-0.02
9	3.30	3.37	-0.07
10	3.10	3.05	+0.05
11	4.16	4.20	-0.04
12	3.51	3.43	+0.08
13	3.53	3.53	+0.00
14	3.54	3.53	+0.01
15	3.53	3.53	+0.00

Table 5. ANOVA test results of acid value for carbon-based magnetic Catalysts.

Source	DF	Adj SS	Adj MS	F-Value	P-Value
Model	09	1.42859	0.158732	029.46	0.0010(S)
Linear	03	1.35982	0.453275	084.12	0.000(HS)
Time (h)	01	0.03781	0.037813	007.02	0.0450(S)
m. /n,Temp (C)	01	0.57781	0.577812	107.23	0.000(HS)
Conc (M)	01	0.74420	0.744200	138.11	0.000(HS)
Square	03	0.01752	0.005839	001.08	0.436
Time (h)*Time (h)	01	0.01293	0.012926	002.40	0.182
Temp(C)*Temp(C)	01	0.00093	0.000926	000.17	0.696
Conc (M)*Conc (M)	01	0.00370	0.003703	000.69	0.445
2-Way Interaction	03	0.05125	0.017083	003.17	0.123
Time (h)*Temp (C)	01	0.00000	0.000000	000.00	1.000
Time (h)*Conc (M)	01	0.00062	0.000625	000.12	0.747
Temp (C)*Conc (M)	01	0.05063	0.050625	009.40	0.028 (S)
Error	05	0.02694	0.005388	—	—
Lack-of-Fit	03	0.02688	0.008958	268.75	0.004
Pure Error	02	0.00007	0.000033	—	—
Total	14	1.45553	—	—	—

Model Summary	R^2	R^2 (adj)	R^2 (pred)
	98.15%	94.82%	70.45%

In this case, concentration is much more influential on acid density than time. It indicates that a higher precursor concentration will enhance the density of acid. Most probably, this is because of an increased availability of sulfuric acid, which contributes to forming sulfonic and other acid functional groups. The third plot evaluates the effect of temperature and concentration interaction with time fixed at 2 hours. These plots exhibit the significant positive effect of temperature and concentration on acid density, and the maximum value was seen at the upper levels of the variables. The surface curvature shows an interaction of a complex type, and the results are that the effect of these two variables on acid density is more complicated than their sole effects. Because the 3D surface plots for these two reactions in the other response surface plots indicate that, with an increase in temperature and concentration, the reaction

generally undergoes improvement in terms of acid density. However, the acid density may reduce at specific temperatures or reaction times with increased reaction time and temperature. This can be due to the thermal decomposition of functional groups containing sulfur or the formation of neutral oxygen and weakly acidic groups at prolonged times. Overall, these 3D surface plots provide valuable insights into the factors influencing the acid density of carbon-based magnetic catalysts, guiding the optimization of synthesis and reaction conditions to achieve desired acid density levels for specific applications.

5. Conclusions

The transesterification process benefits from the use of heterogeneous catalysts derived from natural sources due to their affordability, environmentally friendly properties, and reusability. Consequently, carbon-based solid acids hold significant potential for practical application in biodiesel production as stable and easily separable catalysts. The application of acidic and basic magnetic catalysts demonstrates remarkable catalytic and magnetic efficiency. Heterogeneous magnetic catalysts offer a more efficient method for catalytic separation than conventional heterogeneous solid catalysts, resulting in a higher recovery rate. Initially, palm dust, a waste product, is utilized to produce the carbon support, which is then magnetized and sulfonated to create a carbon-based magnetic catalyst. Iron oxides, essential for the magnetic catalyst, are successfully attached to the catalyst, as confirmed by FTIR analysis. Through the sulfonation process, the -SO3H group is also effectively attached to the amorphous carbon support, as evidenced by FTIR analysis. The manufacturing process results in the successful production of the catalyst. The optimal catalyst is achieved under sulfonation conditions of 50C°, 2.6 hours, and 10 M concentration.

Authors' contribution

All authors contributed equally to the preparation of this article.

Declaration of competing interest

The authors declare no conflicts of interest.

Funding source

This study didn't receive any specific funds.

Data availability

The data that support the findings of this study are available from the corresponding author upon reasonable request.

REFERENCES

[1] Z. Nazzal and A. Jazie, "Green diesel production using egg shell derived cao catalyst: Effect of catalyst and reaction process," *Al-Qadisiyah Journal for Engineering Sciences*, vol. 13, no. 4, pp. 262–267, March 2020. [Online]. Available: http://doi.org/10.30772/qjes.v13i4.697

[2] Z. M. Mezher and H. Mohammed Al.Tameemi, "A catalytic cracking process on atmospheric residue from the al-diwaneyah petroleum refinery," *Al-Qadisiyah Journal for Engineering Sciences*, vol. 15, no. 3, pp. 164–170, 2022. [Online]. Available: https://doi.org/10.30772/qjes.v15i3.829

[3] B. Ang, W. Choong, and T. Ng, "Energy security: Definitions, dimensions and indexes," *Renewable and Sustainable Energy Reviews*, vol. 42, pp. 1077–1093, 2015. [Online]. Available: https://doi.org/10.1016/j.rser.2014.10.064

[4] T.-Z. Ang, M. Salem, M. Kamarol, H. Das, M. Nazari, and N. Prabaharan, "A comprehensive study of renewable energy sources: Classifications, challenges and suggestions," *Energy Strategy Reviews*, vol. 43, p. 100939, 2022. [Online]. Available: https://doi.org/10.1016/j.esr.2022.100939

[5] Q. Hassan, P. Viktor, T. J. Al-Musawi, B. M. Ali, S. Algburi, H. Alzoubi, A. K. Al-Jiboory, A. Z. Sameen, H. Salman, and M. Jaszczur, "The renewable energy role in the global energy transformations," *Renewable Energy Focus*, vol. 48, p. 100545, 2024. [Online]. Available: https://doi.org/10.1016/j.ref.2024.100545

[6] D. Huang, H. Zhou, and L. Lin, "Biodiesel: an alternative to conventional fuel," *Energy Procedia*, vol. 16, no. Part c, pp. 1874–1885, 2012. [Online]. Available: https://doi.org/10.1016/j.egypro.2012.01.287

[7] B. Changmai, C. Vanlalveni, A. Ingle, R. Bhagat, and S. Rokhum, "Widely used catalysts in biodiesel production: a review," *RSC Advances*, vol. 10, pp. 41 625–41 679, 2020. [Online]. Available: https://doi.org/10.26434/chemrxiv.13095551.v2

[8] N. Singh, R. Saluja, H. Rao, R. Kaushal, N. Gahlot, I. Suyambulingam, M. Sanjay, D. Divakaran, and S. Siengchin, "Progress and facts on biodiesel generations, production methods, influencing factors, and reactors: A comprehensive review from 2000 to 2023," *Energy Conversion and Management*, vol. 302, p. 118157, 2024. [Online]. Available: https://doi.org/10.1016/j.enconman.2024.118157

[9] A. Das and S. Rokhum, "Chapter 6 - renewable diesel and biodiesel: a comparative analysis, in: D. kumar, b. singh, s.k. gupta (eds.)," *Renewable Diesel*, pp. 123–166, 2024. [Online]. Available: https://doi.org/10.1016/B978-0-323-91153-5.00002-9

[10] R. Kamaraj, Y. Rao, and B. B, "Biodiesel blends: a comprehensive systematic review on various constraints," *Environmental Science and Pollution Research*, vol. 29, no. 1, p. 43770–43785, 2021. [Online]. Available: https://doi.org/10.1007/s11356-021-13316-8

[11] P. Kalita, B. Basumatary, P. Saikia, B. Das, and S. Basumatary, "Biodiesel as renewable biofuel produced via enzyme-based catalyzed transesterification," *Energy Nexus*, vol. 6, p. 100087, 2022. [Online]. Available: https://doi.org/10.1016/j.nexus.2022.100087

[12] Z. Hussain, M. Haider, M. Tripathi, and R. Kumar, "Catalytic and non-catalytic methods for biodiesel production, in: K.k. pant, s.k. gupta, e. ahmad (eds.)," *Catalysis for Clean Energy and Environmental Sustainability: Biomass*, pp. 185–208, 2021. [Online]. Available: http://doi.org/10.1007/978-3-030-65017-9_7

[13] U. Schuchardt, R. Sercheli, and V. Matheus, "Transesterification of vegetable oils: A review," *Journal of the Brazilian Chemical Society*, vol. 9, no. 3, 1998. [Online]. Available: http://doi.org/10.1590/S0103-50531998000300002

[14] E. Filippi and C. Pizzolitto, "The past and the future of catalysis and technology in industry: a perspective from casale sa point of view," *Catalysis Today*, vol. 387, no. 1, pp. 9–11, 2022. [Online]. Available: https://doi.org/10.1016/j.cattod.2021.11.005

[15] M. Jayakumar, N. Karmegam, M. Gundupalli, K. B. Gebeyehu, B. T. Asfaw, S. Chang, B. Ravindran, and M. K. Awasthi, "Heterogeneous base catalysts: Synthesis and application for biodiesel production – a review," *Bioresource Technology*, vol. 331, p. 125054, 2021. [Online]. Available: https://doi.org/10.1016/j.biortech.2021.125054

[16] S. Krishnan, F. l. Pua, and F. Zhang, "A review of magnetic solid catalyst development for sustainable biodiesel production," *Biomass and Bioenergy*, vol. 149, no. 1, p. 106099, 2021. [Online]. Available: https://doi.org/10.1016/j.biombioe.2021.106099

[17] M. Maquirriain, C. Querini, and M. Pisarello, "Glycerine esterification with free fatty acids: Homogeneous catalysis," *Chemical Engineering Research and Design*, vol. 171, pp. 86–99, 2021. [Online]. Available: https://doi.org/10.1016/j.cherd.2021.04.018

[18] J. Orege, O. Oderinde, G. Kifle, A. Ibikunle, S. Raheem, O. Ejeromedoghene, E. Okeke, O. Olukowi, O. Orege, E. Fagbohun, T. Ogundipe, E. Avor, O. Ajayi, and M. Daramola, "Recent advances in heterogeneous catalysis for green biodiesel production by transesterification," *Energy Conversion and Management*, vol. 258, p. 115406, 2022. [Online]. Available: https://doi.org/10.1016/j.enconman.2022.115406

[19] W. Xie and J. Li, "Magnetic solid catalysts for sustainable and cleaner biodiesel production: A comprehensive review," *Renewable and Sustainable Energy Reviews*, vol. 171, p. 113017, 2023. [Online]. Available: https://doi.org/10.1016/j.rser.2022.113017

[20] A. Akbarzadeh, M. Samiei, and S. Davaran, "Magnetic nanoparticles: preparation, physical properties, and applications in biomedicine," *Nanoscale Research Letters*, vol. 7, no. 144, 2012. [Online]. Available: https://doi.org/10.1186/1556-276X-7-144

[21] S. Basumatary, S. Brahma, M. Hoque, B. Das, M. Selvaraj, S. Brahma, and S. Basumatary, "Advances in cao-based catalysts for sustainable biodiesel synthesis," *Green Energy and Resources*, vol. 1, no. 3, p. 100032, 2023. [Online]. Available: https://doi.org/10.1016/j.gerr.2023.100032s

[22] T. Mabate, N. Maqunga, S. Ntshibongo, M. Maumela, and N. Bingwa, "Metal oxides and their roles in heterogeneous catalysis: special emphasis on synthesis protocols, intrinsic properties, and their influence in transfer hydrogenation reactions," *SN Applied Sciences*, vol. 5, no. 196, 2023. [Online]. Available: https://doi.org/10.1007/s42452-023-05416-6

[23] K. V. Allsburg, E. Tan, J. Super, J. Schaidle, and F. Baddour, "Early-stage evaluation of catalyst manufacturing cost and environmental impact using catcost," *Nature Catalysis*, vol. 5, pp. 342–353, 2022. [Online]. Available: https://doi.org/10.1038/s41929-022-00759-6

[24] A. Umakanth, A. Datta, B. Reddy, and S. Bardhan, "Chapter 3 - biomass feedstocks for advanced biofuels: Sustainability and supply chain management," *in: D. Tuli, S. Kasture, A. Kuila (Eds.)Advanced Biofuel Technologies*, pp. 39–72, 2022. [Online]. Available: https://doi.org/10.1016/B978-0-323-88427-3.00023-4

[25] G. Chutia and K. Phukan, "Biomass derived heterogeneous catalysts used for sustainable biodiesel production: a systematic review," *Brazilian Journal of Chemical Engineering*, vol. 41, pp. 23–48, 2024. [Online]. Available: http://doi.org/10.1007/s43153-023-00371-6

[26] M. Gonçalves, H. Santos, M. da Silva, A. da Cas Viegas, G. da Rocha Filho, and L. da Conceição, "Biodiesel production from waste cooking oil using an innovative magnetic solid acid catalyst based on ni–fe ferrite: Rsm-bbd optimization approach," *Journal of Industrial and Engineering Chemistry*, vol. 135, pp. 270–285, 2024. [Online]. Available: https://doi.org/10.1016/j.jiec.2024.01.038

[27] S. Khan, S. Khan, L. Khan, A. Farooq, K. Akhtar, and A. Asiri, "Fourier transform infrared spectroscopy: Fundamentals and application in functional groups and nanomaterials characterization," *Handbook of Materials Characterization*, pp. 317–344, 2018. [Online]. Available: https://doi.org/10.1007/978-3-319-92955-2_9

[28] C. Liu, P. Lv, Z. Yuan, F. Yan, and W. Luo, "The nanometer magnetic solid base catalyst for production of biodiesel," *Renewable Energy*, vol. 35, no. 7, pp. 1531–1536, 2010. [Online]. Available: https://doi.org/10.1016/j.renene.2009.10.009

[29] M. Brahmayya, S. Dai, and S.-Y. Suen, "Sulfonated reduced graphene oxide catalyzed cyclization of hydrazides and carbon dioxide to 1,3,4-oxadiazoles under sonication," *Scientific Reports*, vol. 7, no. 4675, pp. 341–354, 2017. [Online]. Available: http://doi.org/10.1038/s41598-017-04143-4

[30] S. R. Pouran, A. A. Raman, and W. Daud, "Review on the application of modified iron oxides as heterogeneous catalysts in fenton reactions," *Journal of Cleaner Production*, vol. 64, pp. 24–35, 2014. [Online]. Available: http://doi.org/10.1016/j.jclepro.2013.09.013(2013)

[31] M. Thommes, K. Kaneko, A. Neimark, J. Olivier, F. Rodriguez-Reinoso, J. Rouquerol, and K. Sing, "Physisorption of gases, with special reference to the evaluation of surface area and pore size distribution (iupac technical report)," *Pure and Applied Chemistry*, vol. 87, pp. 1051–1069, 2015. [Online]. Available: https://doi.org/10.1515/pac-2014-1117

[32] J. Gaffney and N. Marley, "Fourier transform infrared (ftir) spectroscopy," *Energy and Buildings*, no. 1, p. 57, 2012. [Online]. Available: https://doi.org/10.1002/0471266965.com107.pub2

[33] F. Tian, Q. Shen, Z. Fu, Y. Wu, and C. Jia, "Enhanced adsorption desulfurization performance over hierarchically structured zeolite y," *Fuel Processing Technology*, vol. 128, no. 6, pp. 176–182, 2014. [Online]. Available: https://doi.org/10.1016/j.fuproc.2014.07.018

[34] O. Amanzadeh, J. Ahmadpour, S. Shabanian, and M. Nikzad, "Experimental, isotherm, kinetic, and thermodynamic studies of the novel modified zeolite zsm-5 adsorbent for use in clean fuel processing," *Chemical Engineering Research and Design*, vol. 203, no. 5, pp. 69–82, 2024. [Online]. Available: https://doi.org/10.1016/j.cherd.2024.01.032

[35] M. Miedaner, R. Weerasooriya, and H. Tobschall, "Chapter 17 - 1-pk modeling strategies for the adsorption of some trace elements onto gibbsite," *J. Lützenkirchen (Ed.) Interface Science and Technology, Elsevier*, vol. 11, pp. 469–490, 2006. [Online]. Available: https://doi.org/10.1016/S1573-4285(06)80061-X

[36] P. Ehiomogue, I. Ahuchaogu, and I. Ahaneku, "Review of adsorption isotherms models," *ACTA TECHNICA CORVINIENSIS – Bulletin of Engineering Tome XIV*, no. 8, p. 79–87, 2022.

How to cite this article:
Ali Flayyih Hasan, Ahmed A. Obaid, Omid Amanzadeh, and Falah Abdulhassan (2025). 'Synthesis and study of carbon-based magnetic catalysts for biodiesel production', Al-Qadisiyah Journal for Engineering Sciences, 18(3), pp. 281-289. `https://doi.org/10.30772/qjes.2024.150386.1259`